Published OnlineFirst January 16, 2014; DOI: 10.1158/1535-7163.MCT-13-0748

Large Molecule Therapeutics

Molecular Cancer Therapeutics

Enhancement of the Tumor Penetration of Monoclonal Antibody by Fusion of a Neuropilin-Targeting Peptide Improves the Antitumor Efficacy

Tae-Hwan Shin[1], Eun-Sil Sung[1], Ye-Jin Kim[1], Ki-Su Kim[3], Se-Ho Kim[3], Seok-Ki Kim[4], Young-Don Lee[2], and Yong-Sung Kim[1]

Abstract

The limited localization and penetration of monoclonal antibodies (mAb) into solid tumors restricts their antitumor efficacy. Here, we describe a solid tumor–targeting antibody with enhanced tumor penetration activity. We designed a 22-residue peptide (A22p), which was extracted from the C-terminal basic region of semaphorin 3A (Sema3A) but modified to have higher affinity with neuropilin receptors (NRP), and genetically fused it to the C-terminus of Fc of human immunoglobulin G1 via a 15-residue $(G_4S)_3$ linker, generating Fc-A22p, for the bivalent binding to NRPs. In contrast to Fc or the monovalent A22p peptide alone, Fc-A22p homed to tumor vessels and induced vascular permeability through VE-cadherin downregulation and penetrated tumor tissues by interacting with NRPs in mice bearing human tumor xenografts. We extended the Fc-A22p platform by generating mAb-A22p antibodies of two clinically approved solid tumor–targeting mAbs, the anti-EGF receptor mAb cetuximab (erbitux), and the anti-Her2 mAb trastuzumab (herceptin). The mAb-A22p antibodies retained the intrinsic antigen binding, natural Fc-like biophysical properties, and productivity in mammalian cell cultures, comparable with those of the parent mAbs. In mouse xenograft tumor models, the mAb-A22p antibodies more efficiently homed to tumor vessels and spread into the extravascular tumor parenchyma, which significantly enhanced antitumor efficacy compared with the parent mAbs. Our results suggest that mAb-A22p is a superior format for solid tumor–targeting antibodies due to its enhanced tumor tissue penetration and greater antitumor efficacy compared with conventional mAbs. *Mol Cancer Ther; 13(3); 651–61. ©2014 AACR.*

Introduction

Poor localization and penetration of monoclonal antibodies (mAb) into solid tumors is one of main mechanisms of limiting tumor response to antibody therapy (1, 2). For example, mAb accumulation in tumors of patients is typically very inefficient, in the order of 0.001% to 0.01% of the injected dose per gram of tumor (2–4). For anticancer mAbs targeting antigens expressed on solid tumors, systemically administered mAbs need to selectively localize to tumor vessels, cross the blood vessels into the tumor parenchyma, and then penetrate into tumor tissues across the interstitium by diffusion or convection to reach as many tumor cells as possible (2–4). However, the abnormal physiologic and physical properties of solid tumors, such as the defective blood vessels, lack of lymphatic drainage, and extracellular matrix components, limit the extravasation of mAbs from blood vessels and spread within tumor tissues (3–5). In addition, the intrinsic properties of mAbs, including the relatively large size (approximately 150 kDa) and high-affinity antigen binding, may restrict vascular extravasation and transport within tumor tissue (3, 5).

Several antibody-engineering approaches have been used to improve the tumor tissue penetration of mAbs, including manipulations of molecular size, charge, valency, and antigen-binding affinity (6). Another approach includes the coadministration of mAbs with so-called promoter agents that enhance vascular permeability and/or reduce epithelial barriers, which leads to improved tumor tissue penetration of blood-borne mAbs (reviewed in refs. 2, 5). For example, coadministration of an internalizing Arg–Gly–Asp (iRGD) tumor-penetrating peptide (7–9) and a viral protein called epithelial junction opener-1 (JO-1; ref. 10) significantly enhanced tumor penetration and antitumor efficacy of the anti-Her2 mAb trastuzumab (Herceptin) and the anti-EGF receptor (EGFR) mAb

Authors' Affiliations: [1]Department of Molecular Science and Technology, Ajou University; [2]Department of Anatomy, Ajou University School of Medicine, Suwon; [3]Antibody Engineering Team, Mogam Biotechnology Research Institute, Yongin; and [4]Molecular Imaging and Therapy Branch, National Cancer Center, Goyang, Korea

Note: Supplementary data for this article are available at Molecular Cancer Therapeutics Online (http://mct.aacrjournals.org/).

Corresponding Author: Yong-Sung Kim, Ajou University, 206 Worldcup-ro, Suwon, 443-749, Korea. Phone: 82-31-219-2662; Fax: 82-21-219-1610; E-mail: kimys@ajou.ac.kr

doi: 10.1158/1535-7163.MCT-13-0748

Published OnlineFirst January 16, 2014; DOI: 10.1158/1535-7163.MCT-13-0748

cetuximab (Erbitux), respectively, in mouse xenograft tumor models.

In this study, we sought to develop a format of solid tumor–targeting antibody with enhanced vascular extravasation and tumor penetration activity. We achieved this by fusing mAbs to a tumor-penetrating peptide that targets tumor-associated proteins. For the target protein, we chose a neuropilin receptor (NRP) because NRPs are abundantly expressed on the surface of many tumor endothelial and epithelial cells (11) and can increase vascular permeability upon activation by their intrinsic ligands (12, 13). Further, some NRP-binding peptides have been shown to improve tumor tissue penetration of coadministered anticancer drugs, including mAbs (8, 14). Human NRP1 and NRP2 (NRP1/2), which share 44% sequence identity, are coreceptors of plexin receptors for secreted class 3 semaphorin (Sema3) ligands, and are coreceptors of VEGF receptors (VEGF-R) for VEGF ligands (11, 15). In addition to the ligand-specificity determining a1a2 domains, NRP1/2 have a specific C-terminal arginine-binding pocket on the b1 domain, which is the shared binding site for furin-processed Sema3 and VEGF ligands with a C-terminal Arg residue (see Supplementary Fig. S1A–S1C for details; refs. 16, 17) and for peptides with Arg/Lys-rich C-terminal motifs (9, 18).

Sema3A, a prototype Sema3 ligand, increases vascular permeability (12). However, unlike VEGF, Sema3A suppresses VEGF-mediated angiogenesis and induces tumor vascular normalization (19, 20). Therefore, we designed an NRP-targeting 22-mer peptide (A22p) based on the C-terminal basic tail of Sema3A, but we modified it to have higher affinity for NRPs. When A22p was genetically fused to the C-terminus of Fc to generate Fc-A22p and administered, we found that Fc-A22p induced vascular permeability and penetrated into tumor tissues by interacting with NRPs. We further explored the Fc-A22p platform with 2 clinically available solid tumor–targeting mAbs, the anti-EGFR cetuximab, and the anti-Her2 trastuzumab. We demonstrated that administration of these 2 mAbs as mAb-A22p antibodies improved tumor tissue penetration and antitumor efficacy in xenograft tumor models compared with the parent mAbs, providing a superior antibody format for solid tumor therapy.

Materials and Methods

Cell lines

Human umbilical vein endothelial cells (HUVEC) purchased from Innopharmascreen were maintained in complete endothelial growth medium-2 (EGM-2; PromoCell) and, if necessary, starved in endothelial basal medium-2 (EBM-2; PromoCell). HUVECs at passages from 3 to 8 were used throughout the study. Human cancer cell lines, SK-OV-3 (Ovary), A431 (Epidermis), and FaDu (Pharynx) cells were purchased from Korean Cell Line Bank where they were characterized by DNA fingerprinting. SK-OV-3 and A431 cell lines were cultured in RPMI1640 (Welgene; ref. 21). FaDu cell lines were cultured in Minimum Essential Media (MEM; Welgene). PPC-1 cell lines were obtained from Prof. Keesook Lee (Chonnam National University, Korea) and cultured in Dulbecco's modified eagle media (DMEM; Welgene; ref. 22). Media were supplemented with 10% (v/v) heat inactivated FBS (Welgene), 100 units/mL of penicillin, and 100 μg/mL of streptomycin (Welgene). All of the cell lines were maintained at 37°C in a humidified 5% CO_2 incubator and routinely screened for *Mycoplasma* contamination (CellSafe).

Construction, expression, and purification of antibodies

DNA encoding human immunoglobulin G1 (IgG1) Fc (hinge-CH2-CH3, residues 225–447 in EU numbering) was subcloned into pcDNA3.4 vector (Invitrogen) for Fc expression (23). The heavy and light chains of the anti-EGFR mAb cetuximab (24) and the anti-Her2 mAb trastuzumab (25) were subcloned into pcDNA3.4 vector (Invitrogen) using a combination of gene synthesis and overlapping PCR. Fc-A22/-A22p or mAb-A22p was constructed by cloning the peptide and $(G_4S)_3$ linker in frame at the end of the Fc. Antibodies were produced by transient transfection of the plasmids into HEK293F cells using the Freestyle 293-F expression and media system (Invitrogen), as we described before (23). Antibodies were purified from the culture supernatants using a Protein-A agarose chromatography column (GE Healthcare; ref. 26).

Confocal immunofluorescence microscopy of cells

Confocal immunofluorescence microscopic analyses were performed as described (27). Cells (5×10^4 cells/well) grown overnight on coverslips in 24-well culture plates were washed, incubated in serum-free transfection optimized medium (TOM; Welgene) for 30 minutes at 37°C, and then treated with proteins diluted in TOM medium at 37°C for the indicated periods. After washed 2 times with cold PBS, cells were fixed with 2% paraformaldehyde in PBS for 10 minutes at 25°C, and then permeabilized with Perm buffer [0.1% saponin, 0.1% sodium azide, 2% bovine serum albumin (BSA) in PBS] for 10 minutes at 25°C. After blocking with 2% BSA in PBS for 1 hour at 25°C, internalized proteins were detected with fluorescein isothiocyanate (FITC)-conjugated anti-human IgG for 1 hour at 25°C. In the colocalization assay with NRP1 or NRP2, the primary anti-human/mouse/rat/monkey NRP1 (Abcam) or anti-human/mouse/rat NRP2 antibody (Santa Cruz Biotechnology) was additionally incubated overnight at 4°C before the detection with the secondary antibody tetramethylrhodamine (TRITC)-conjugated anti-rabbit IgG (Sigma) for 1 hour at 25°C. After mounting the coverslips onto glass slides with VECTASHIELD [mounting medium with 4′,6-diamidino-2-phenylindole (DAPI), Vector Laboratories], optical confocal sections were obtained on a Zeiss LSM710 systems with the ZEN software (Carl Zeiss).

Published OnlineFirst January 16, 2014; DOI: 10.1158/1535-7163.MCT-13-0748

Endothelial permeability assay

Permeability across endothelial cell monolayers was assessed using HUVECs as previously described (13, 28). Briefly, HUVECs or siRNA-transfected HUVECs (5×10^4 cells/well) were seeded into the 12-well Transwell chamber (0.4-μm pore size; Corning Coster Corp) and grown for 3 days to form mature monolayers. After 4 hours of serum starvation of the cells, Fc proteins (1 μmol/L), VEGF165 (1.3 nmol/L ≈ 50 ng/mL), or Sema3A (1.3 nmol/L ≈ 220 ng/mL) were added to the upper chamber. After 30 minutes, 50 μg of FITC-conjugated dextran (approximately 40 kDa, 1 mg/mL; Sigma) was treated to the upper chamber. After 30 minutes, each sample from the bottom chamber was measured in triplicate on a fluorescent plate reader (Molecular Devices). Data were normalized to PBS-treated samples.

Xenograft tumor models

All animal experiments were evaluated and approved by Animal and Ethics Review Committee of Ajou University (Suwon, Korea) and done according to the guidelines established by the Institutional Animal Care and Use Committee. Female BALB/c athymic nude mice (NARA Biotech), ages 4 weeks and weighed between 15 and 20 g, were inoculated subcutaneously with FaDu (5×10^6 cells/mouse), A431 (5×10^6 cells/mouse), or SK-OV3 (1×10^7 cells/mouse) cells in the right thigh. When the mean tumor size reached 80 to 120 mm^3 (after 5–7 days growth), mice were randomized into each groups ($n = 7$ per group) and administered intravenously via tail vein in a dose/weight-matched fashion every 3 days (total, 6 times) with proteins or antibodies, as specified in the figure legends. Tumor length and width were measured every 3 days using calipers, and tumor volumes were calculated by the formula $^1/_2 \times \text{length} \times \text{width}^2$ (26). The statistical significance was evaluated by one-way analysis followed by two-tailed Student *t* tests on Excel Software (Microsoft Inc.).

Immunofluorescence of tumor tissues

A single dose of Fc proteins (2.5 mg/kg), antibodies (2.5 mg/kg), or biotinylated A22 or A22p peptides (5 mg/kg) was intravenously injected into mice bearing FaDu, SK-OV3, or A431 xenografted tumors with an average size of approximately 7 to 8 mm in diameter. Tumor tissues were harvested 3 or 12 hours postinjection. The preparation of tumor tissue section and immunofluorescence staining of the cryosections were performed as described before (29, 30). Briefly, the excised tumors from mice were fixed in 4% paraformaldehyde overnight at 4°C, cryoprotected in 30% sucrose for 10 hours, and then frozen in optimum cutting temperature (OCT; Tissue-Tek) embedding medium. For immunofluorescence staining, cryosections were prepared at 10 μm thickness and incubated with blocking solution (2% BSA in PBS) for 1 hour at 25°C. Tissue sections were stained with FITC-conjugated anti-human IgG (Sigma) in 2% BSA in PBS for 1.5 hours at 25°C in dark to detect Fc proteins or antibodies, and then washed 3× with PBST (PBS with 0.1% Tween 20; 10 minutes each wash). After another blocking step with blocking solution (2% BSA in PBS) for 1 hour at 25°C, tissue sections were also stained with rat anti-mouse CD31 mAb, rabbit anti-human/mouse/rat NRP1 (Abcam), or rabbit anti-human/mouse/rat/monkey NRP2 antibody (Santa Cruz Biotechnology) in 2% BSA in PBS at 4°C overnight, washed 3× with PBST and then stained with goat anti-rat TRITC-conjugated antibodies (Millipore), FITC-conjugated anti-human IgG Fc antibody, or streptavidin-FITC (Invitrogen) at 25°C for 1.5 hours in dark. Slides were then washed 3× with PBST and then mounted in VECTASHIELD. Tissue sections were examined by Ziess LSM710 systems with the ZEN software (Carl Zeiss). Fluorescence images in each tissue were quantified for positive area of Fc- or streptavidin (SA)-staining with the ImageJ software (NIH).

In vivo permeability assay

Female BALB/c athymic nude mice bearing preestablished FaDu tumor (about 1 cm in diameter) were injected intravenously with Fc proteins (150 μg), VEGF165 (400 ng), and Sema3A (400 ng) combined with 1 mg of Evans Blue (Sigma) in PBS. After 40 minutes of circulation, the mice were perfused through the heart with PBS containing 1% BSA, and tumors were collected ($n = 3$ per group). For Evans Blue quantification, the dye was extracted from tumors in 1 mL of 2,2,-*N*-methylformamide (Sigma) for overnight at 37°C with mild shaking and quantified by measuring the absorbance at 600 nm with a spectrophotometer (8).

Statistical analysis

Data are reported as the mean ± SD of at least 3 independent experiments, unless otherwise specified. Comparison between two groups was analyzed for statistical significance by a two-tailed unpaired Student *t* test in Sigma Plot 8.0 software (SPSS Inc.). A *P* value of less than 0.05 was considered statistically significant.

Details of reagents, recombinant protein expression and purification, construction, expression, and purification of antibodies, binding analysis by ELISA, surface plasmon resonance (SPR), flow cytometric analysis, cell proliferation assay, Western blotting and immunoprecipitation, colocalization studies by confocal immunofluorescence microscopy, RNA interference, and *ex vivo* tumor penetration assays are given in the Supplementary Materials and Methods.

Results

Design and generation of high-affinity NRP-binding Fc-A22p

To find an NRP-targeting peptide among human proteins, we analyzed the interactions between NRPs and their intrinsic ligands. Sema3A, as a disulfide-linked homodimer, interacts with two molecules each of NRP1

Published OnlineFirst January 16, 2014; DOI: 10.1158/1535-7163.MCT-13-0748

and plexinA1 for cellular signaling (Supplementary Fig. S1C; ref. 11). The C-terminal basic tail of furin-processed Sema3A is believed to bind to a cleft with negative charge in the b1 domain of NRPs, so-called C-terminal arginine-binding pocket (17, 31), as does the exon 8-encoded domain of VEGF165 (16). Guided by the recent crystal structure of VEGF165/NRP1-b1 domain (32), we chose the C-terminal 22 residues of Sema3A (called A22), corresponding to residues 739–760 (31), as a targeting moiety for the C-terminal arginine-binding pocket of both NRP1 and NRP2 (Supplementary Fig. S1D). The A22 peptide was genetically fused to the C-terminus of human IgG1 Fc via a 15-residue $(G_4S)_3$ linker, generating Fc-A22 (Fig. 1A), which was intended to mimic the bivalent binding of Sema3 ligands to NRP1/2 (Fig. 1B).

Fc-A22 purified from HEK293F cell cultures bound to soluble b1b2 domains of NRPs (NRP-b1b2) with affinity in the micromolar range (K_D = approximately 6–9 μmol/L; Supplementary Fig. S2A), which was approximately 200-fold lower than that of Sema3A (Fig. 1C; Supplementary Table S1). To increase the binding affinity, we designed another peptide, called A22p, with the same sequence as A22 except for an Asn to Pro substitution (N758P) at the third residue from the C-terminus based on structural analysis of the VEGF165/NRP1-b1 domain (Fig. 1A; ref. 32). VEGFs with a conserved Pro residue at this position instead of the Asn in Sema3s have an approximately 10-fold higher affinity for NRPs (Supplementary Fig. S1D and Supplementary Table S1). Fc-A22p, which was constructed in the same way as Fc-A22 (Fig. 1A), was well expressed in the correctly assembled form in HEK293F cell cultures (Supplementary Fig. S2B and Supplementary Table S2). Fc-A22p bound to both NRP1-b1b2 and NRP2-b1b2 domains with an approximately 100-fold higher affinity (K_D = approximately 63 nmol/L) than that of Fc-A22 (Fig. 1C; Supplementary Table S1). In contrast, the synthesized A22p peptide alone bound very weakly to NRP-b1b2 even at 10 μmol/L (Fig. 1C), suggesting that the bivalent binding format of Fc-A22p is critical for high-affinity

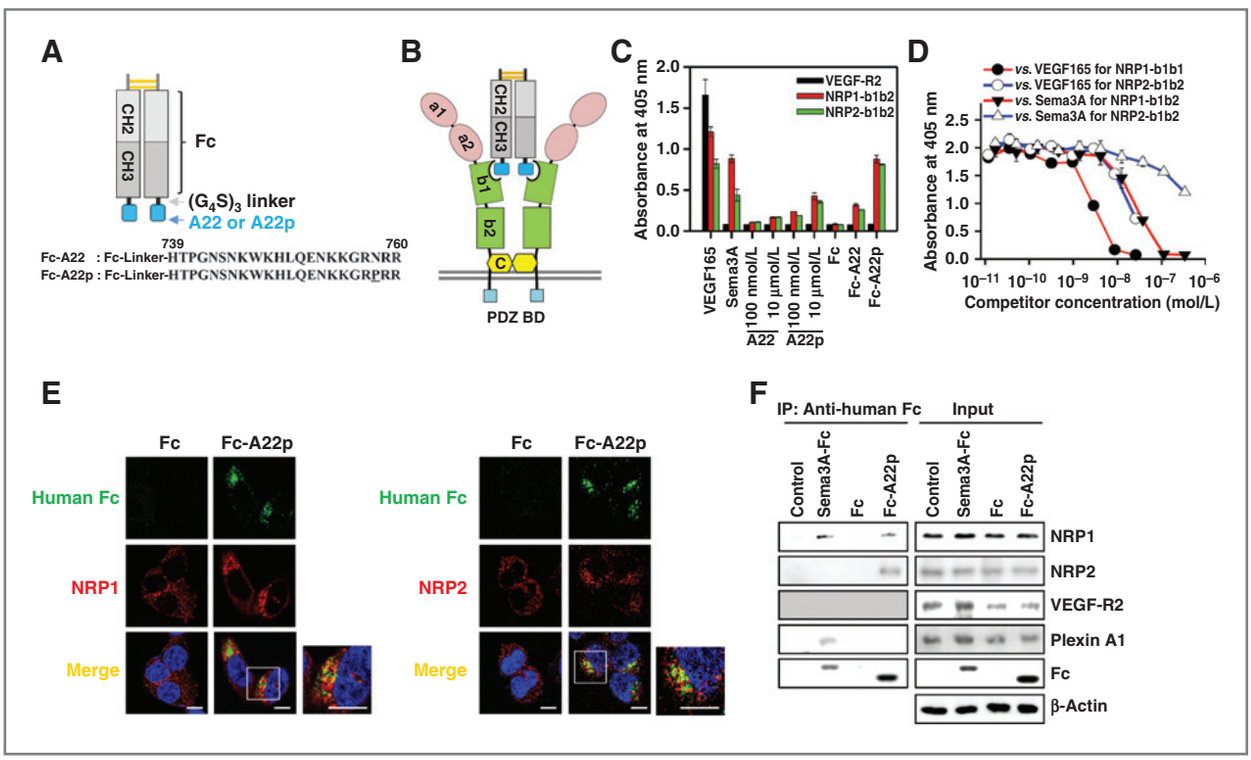

Figure 1. Generation and characterization of high-affinity NRP-binding Fc-A22p. A, schematic diagram of the Fc-A22 and Fc-A22p constructs, in which the A22 (residues 739–760 of Sema3A) or A22p peptide with N758P substitution (underlined) was fused via a 15-residue $(G_4S)_3$ linker to the C-terminus of human IgG1 Fc. B, a hypothetical model showing the bivalent binding of Fc-A22/A22p to NRPs via the interaction of the C-terminal NRP-targeting peptide with the arginine-binding pocket in the b1 domain of NRPs. Details of NRP domains are described in Supplementary Fig. S1A. C, direct ELISA to determine the binding specificity of the indicated Fc protein (100 nmol/L) or synthesized A22 and A22p peptide (100 nmol/L and 10 μmol/L) to plate-coated NRP1-b1b2, NRP2-b1b2, or VEGF-R2-Fc. VEGF165 (100 nmol/L) and Sema3A (100 nmol/L) were employed as controls. D, competitive ELISA of Fc-A22p (30 nmol/L) with increasing concentrations of VEGF165 or Sema3A for binding to plate-coated NRP1-b1b2 or NRP2-b1b2. In C and D, error bars, ±SD. E, internalization of Fc-A22p (green) and its colocalization with NRP1 and NRP2 (red) in HUVECs, determined by confocal fluorescence microscopy. The cells were treated with 1 μmol/L Fc or Fc-A22p at 37°C for 30 minutes. Nuclei were costained with DAPI (blue). Right, enlarged images of the boxed region on the left. Image magnification, ×400; scale bars, 10 μm. F, Western blot analysis of immunoprecipitation (IP) using an anti-human Fc antibody for the lysates of HUVECs, which were untreated (control) or treated with Sema3A-Fc (18 nmol/L), Fc (1.5 μmol/L), or Fc-A22p (1.5 μmol/L) for 0.5 hour. Equal precipitates were analyzed by Western blotting with β-actin as a loading control.

Published OnlineFirst January 16, 2014; DOI: 10.1158/1535-7163.MCT-13-0748

binding due to the avidity effect. Fc-A22p did not cross-react with soluble VEGF-R2 protein (Fig. 1C), but competed with VEGF165 and Sema3A for binding to both soluble NRP-b1b2 (Fig. 1D) and cell surface–expressed NRPs in human ovarian cancer SK-OV-3 cells (Supplementary Fig. S3B). This indicates that Fc-A22p specifically binds to NRPs, particularly to the arginine-binding pocket in the NRP-b1 domain.

Fc-A22p specifically interacts with NRPs undergoing cellular internalization

Cellular internalization of NRP1/2 in response to their intrinsic ligands, such as VEGF165 and Sema3A, is essential for triggering intracellular signaling (14, 33). When Fc-A22p was incubated at 37°C for 30 minutes with HUVECs and SK-OV-3 tumor cells, it was internalized into the cells and colocalized with NRP1 and NRP2 as well as the early endosomal marker EEA1 (Fig. 1E; Supplementary Fig. S3C and S3D), suggesting that Fc-A22p may act as an agonist to NRPs (9). However, Fc-A22p did not cause any significant cytotoxicity on NRP1/2-expressing HUVECs, SK-OV-3, FaDu, and A431 cells during 72-hour incubation (Supplementary Fig. S4).

We further analyzed the molecular components that interact with Fc-A22p by immunoprecipitating Fc-A22p from cell lysates of Fc-A22p–treated HUVECs, and compared it with Fc and Sema3A. Sema3A physically interacted with NRP1 and plexinA1, but not with NRP2 or VEGF-R2 (Fig. 1F), confirming the ligand binding specificity on the cell surface (13). However, Fc-A22p pulled down NRP1 and NRP2, but not VEGF-R2 or plexinA1 (Fig. 1F), suggesting that Fc-A22p only binds to NRPs.

Fc-A22p homes to tumor vessels and penetrates extravascular tumor tissues

Human head and neck squamous carcinoma FaDu cells express both NRP1 and NRP2 (Supplementary Fig. S3A). Mouse and human NRP1 and NRP2 share high sequence homology (93% and 95%, respectively; ref. 14), particularly with 100% conserved the C-terminal arginine-binding pocket in the b1 domain (17). To determine whether Fc-A22p localizes to and penetrates into tumors, a single dose of Fc-A22p was injected intravenously into mice with preestablished FaDu tumors. After 3 and 12 hours of circulation, tumors were excised and sectioned, and then the localization of Fc proteins in relation to blood vessels was determined by immunofluorescence staining. Compared with Fc, Fc-A22p was significantly detected in and around tumor vessels as early as after 3 hours of circulation and after 12 hours of circulation and it was even inside the tumor tissue far from the vessels (Fig. 2A). Quantification of the Fc protein–positive areas revealed that the distribution of Fc-A22p in the tumor tissues was more than 2-fold higher than that of Fc. Fc-A22p was colocalized with NRP1/2 on the tumor vessels and tissues in which

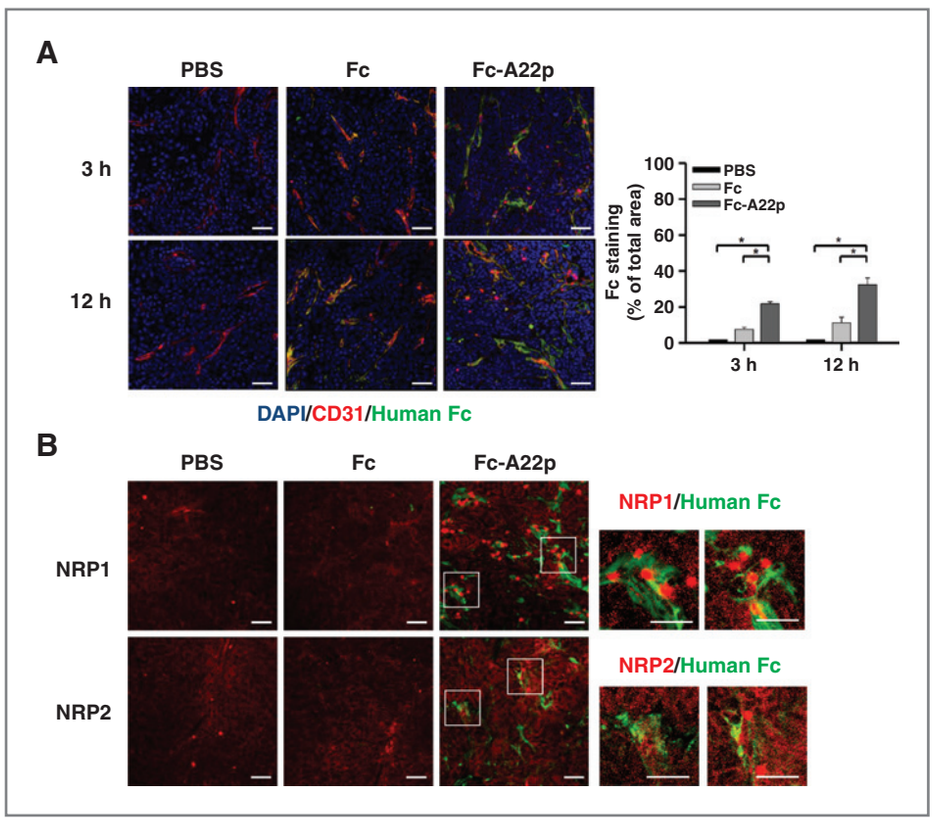

Figure 2. Fc-A22p exhibits rapid tumor homing, improved extravasation, and colocalization with NRPs. A and B, representative images showing the distribution of intravenously injected Fc (2.5 mg/kg) or Fc-A22p (2.5 mg/kg) in relation to blood vessels (A) and colocalization with NRP1/2 within tumor tissue (B) in FaDu xenograft mice, determined by immunofluorescence staining. In A, after Fc proteins were circulating for 3 or 12 hours, tumor tissues were excised and stained for human Fc (FITC, green) and CD31 (TRITC, red). Blue represents DAPI staining. Right, the quantification of positive areas of Fc-staining (green) analyzed by the ImageJ software. Results are the mean ±SD of four fields per tumor ($n = 3$ per group). *, $P < 0.05$. In B, after the Fc proteins were circulating for 12 hours, tumor tissues were excised and stained for human Fc (FITC, green) and human/mouse NRP1 or NRP2 (TRITC, red). Right, enlarged images of the boxed regions on the left. Image magnification, ×200; scale bar, 50 μm.

Published OnlineFirst January 16, 2014; DOI: 10.1158/1535-7163.MCT-13-0748

NRP1 and NRP2 were abundantly expressed (Fig. 2B). Similar results were obtained in mice bearing human epidermoid carcinoma A431 xenografts (Supplementary Fig. S5A). Fc-A22, which has the lower-affinity A22 peptide fused to Fc, also exhibited tumor homing and penetration at 3 hours postinjection, but less efficiently than Fc-A22p. In contrast, the monovalent A22 and A22p peptides were not detected in the tumor tissues (Supplementary Fig. S5A).

Fc-A22p enhances vascular permeability in endothelial cells through NRP-dependent downregulation of vascular endothelial cadherin

The efficient extravasation of Fc-A22p in the xenografted tumors prompted us to determine whether Fc-A22p increases vascular permeability in an *in vitro* transendothelial permeation assay using HUVECs. Fc-A22p enhanced passage of FITC–dextran through HUVEC monolayers by more than 3-fold, and was similar to that of VEGF165 and Sema3A, whereas the Fc-mediated enhancement was negligible (Fig. 3A). NRP1/2 knockdown by siRNAs demonstrated that the induced endothelial permeability of Fc-A22p was dependent on NRP1/2 (Fig. 3A). The ability of Fc-A22p to induce tumor vascular permeability was further assessed *in vivo* by the extravasation of Evans blue dye coinjected intravenously into mice bearing FaDu tumors. Similarly to the well-known vascular permeability-inducing ligands Sema3A and VEGF165 (12, 13), coadministration of Fc-A22p increased the accumulation of Evans blue dye in tumors by approximately 2-fold compared with coadministration of Fc (Fig. 3B).

Vascular endothelial (VE)-cadherin acts as endothelial barrier by maintaining adherent junctions between cells, and its downregulation is closely correlated with cell–cell junction destabilization and elevated endothelial permeability (12). Treatment of Fc-A22p, but not Fc, downregulated VE-cadherin in HUVECs in an NRP1/2-dependent manner to levels similar to those of VEGF165 and Sema3A (Fig. 3C and D; refs. 12, 19, 20). The A22 and A22p peptides had no effects, and Fc-A22 had a lesser effect than Fc-A22p on VE-cadherin downregulation and transendothelial permeability in HUVECs (Supplementary Fig. S5B and S5C). Like VEGF165 stimulation in HUVECs, Fc-A22p, but not Fc, markedly reduced the amount of VE-cadherin in the cell

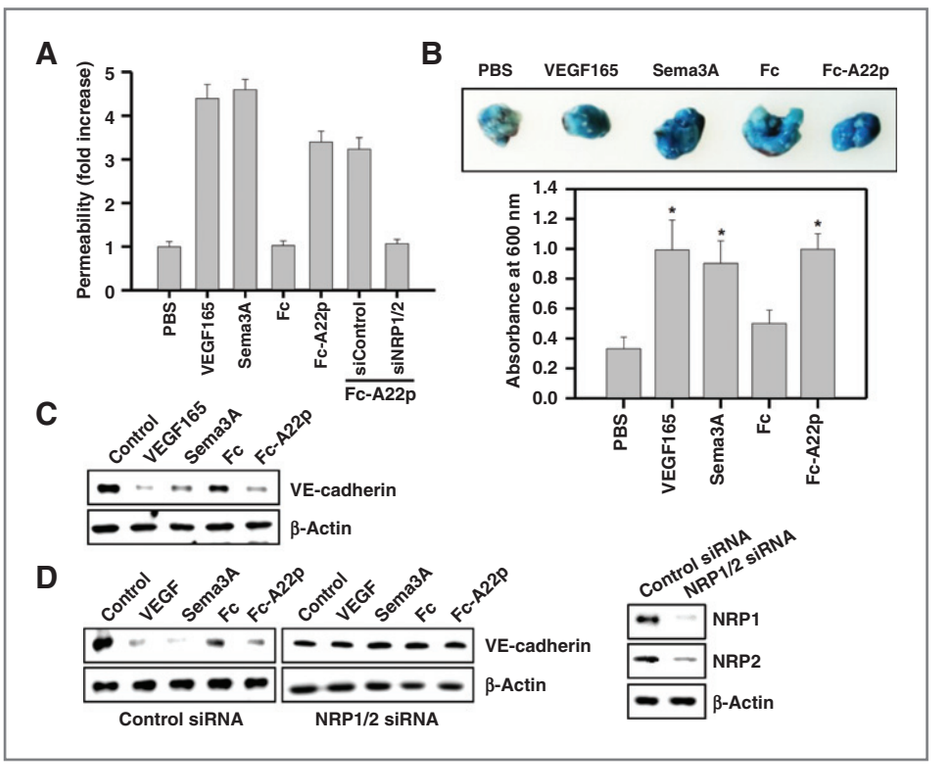

Figure 3. Fc-A22p induces vascular permeability through NRP1/2-dependent downregulation of VE-cadherin. A, permeability across a HUVEC monolayer was assessed by FITC–dextran passage after the cells were stimulated for 30 minutes with VEGF165 (1.3 nmol/L), Sema3A (1.3 nmol/L), Fc (1 μmol/L), or Fc-A22p (1 μmol/L). Data, mean ±SD of the fold increase over PBS-treated cells. B, macroscopic tumor images showing Evans blue dye accumulation (top) and quantification in tumor tissues ($n = 3$ per group; bottom), induced by intravenous coinjection of Evans blue with PBS, VEGF165 (400 ng), Sema3A (400 ng), Fc (150 μg), or Fc-A22p (150 μg) into FaDu xenograft mice. Error bars, ±SD. *, $P < 0.01$ versus the PBS-treated control group. C and D, Western blots showing VE-cadherin levels in HUVECs (C) or NRP1/2-knocked down HUVECs (D), treated for 10 minutes with basal medium (control), VEGF165 (1.3 nmol/L), Sema3A (1.3 nmol/L), Fc (1 μmol/L) or Fc-A22p (1 μmol/L). In A and D, HUVECs were transfected with a scrambled siRNA (control) or cotransfected with NRP1 and NRP2 siRNAs (NRP1/2 siRNA) for 30 hours before treatment.

Published OnlineFirst January 16, 2014; DOI: 10.1158/1535-7163.MCT-13-0748

periphery and its colocalization with F-actin (Supplementary Fig. S6A), suggesting the opening of endothelial cell–cell contacts (34). Therefore, these results mirror those of the *in vivo* tumor extravasation assay (Fig. 3B; Supplementary Fig. S5).

Fc-A22p induces NRP-mediated E-cadherin downregulation in tumor cells and penetrates *ex vivo* tumor tissues

Because many tumor cells overexpress NRPs on their cell surface (Supplementary Fig. S3A; ref. 11), we assessed the effects of Fc-A22p on E-cadherin, an epithelium-specific cell adhesion molecule, in tumor cells. E-cadherin is a principal component of the adherens junctions and is of particular importance to the limited tissue penetration of mAbs (4). Fc-A22p noticeably downregulated E-cadherin in FaDu and A431 cells in an NRP1/2-dependent manner (Fig. 4A and B) and disrupted the integrity of cell–cell junctions (Supplementary Fig. S6B). However, Fc-A22p neither upregulated N-cadherin nor downregulated β-catenin, signaling involved in tumor invasion and metastasis (35, 36). The monovalent peptides A22 and A22p did not affect E-cadherin levels in A431 cells (Supplementary Fig. S5D).

The ability of Fc-A22p to downregulate E-cadherin prompted us to investigate whether Fc-A22p can actively penetrate into *ex vivo* tumor tissues. FaDu xenografts were excised from mice and incubated with Fc proteins for 2.5 hours at 37°C. Analysis of tumor sections revealed that Fc-A22p, but not Fc, penetrated more than 4 to 5 cell layers deep in 2.5 hours into the xenograft explants (Supplementary Fig. S5E), indicative of the relationship between tumor penetration activity and E-cadherin downregulation.

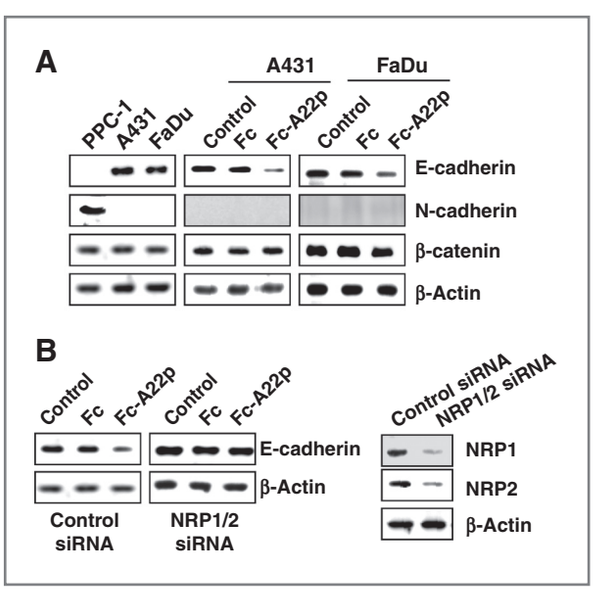

Figure 4. Fc-A22p downregulates E-cadherin in an NRP1/2-dependent manner in tumor cells. A and B, Western blots showing the levels of E-cadherin, N-cadherin, and β-catenin in A431 and FaDu cells (A) and E-cadherin in NRP1/2-knocked down FaDu cells (B), treated for 10 minutes with medium (control), Fc (1 μmol/L), or Fc-A22p (1 μmol/L). PPC-1 cells expressing N-cadherin were used for an antibody control (left). In B, the cells were transfected with the indicated siRNA for 30 hours before the protein treatments.

mAb-A22p antibodies bind to NRPs while retaining the intrinsic antigen-binding and Fc properties of the parent mAbs

To test the Fc-A22p platform for solid tumor–targeting mAbs, A22p was fused via a 15-residue $(G_4S)_3$ linker to the C-terminus of the heavy chain of 2 clinically approved solid tumor–targeting mAbs, the anti-EGFR cetuximab (chimeric IgG1) and the anti-Her2 trastuzumab (humanized IgG1), generating mAb-A22p antibodies (cetuximab-A22p and trastuzumab-A22p, respectively; Fig. 5A). Expression of mAb-A22p antibodies by transient transfection into HEK293F cells yielded similar production levels to those of the parent mAbs (Supplementary Fig. S7A and Supplementary Table S2). The mAb-22p antibodies maintained their respective specific antigen-binding affinity and exhibited simultaneous binding to both the target antigen and the NRP-b1b2 domain (Supplementary Fig. S7B and Supplementary Table S3). When incubated at 37°C with EGFR-negative, NRP1-expressing PPC-1 human prostate tumor cells, cetuximab-A22p was internalized into the cells and colocalized with NRP1, which was not observed with the parent cetuximab (Supplementary Fig. S7C). Therefore, mAb-A22p can trigger NRP-mediated cellular internalization, which is indicative of NRP activation by mAb-A22p, as was observed with Fc-A22p (Fig. 1E). Cetuximab-A22p exerted comparable inhibitory effects on the cell proliferation and EGFR activation to those of cetuximab, indicative of a neutral role of A22p in the *in vitro* biologic activities of cetuximab-A22p (Supplementary Fig. S8). The mAb-A22p maintained the typical pH-dependent binding property for neonatal Fc receptor (FcRn; Supplementary Fig. S7D and Supplementary Table S3), which plays an important role in maintaining the serum half-lives of antibodies. The affinities of mAb-A22p binding to FcγRIIa, FcγRIIIa, and FcγRIIIb were also comparable with those of the parent mAbs (Supplementary Table S3).

mAb-A22p antibodies exhibit enhanced tumor homing and extravascular tumor penetration

We compared the tumor homing and intratumoral distribution of mAb-A22p with those of the parent mAbs by intravenously injecting them into mice harboring EGFR-overexpressing FaDu xenografts for cetuximab and Her2-overexpressing SK-OV-3 xenografts for trastuzumab and then immunofluorescent staining the tumor sections at 3 and 12 hours postinjection. The intratumoral accumulation and penetration of the mAbs increased with circulation time (Fig. 5B; Supplementary Fig. S9A), in agreement with previous results (29, 30). After equivalent circulation times, more noticeable extravasation and farther spreading from the blood vessels in tumor tissues was observed with the mAb-A22p antibodies, approximately

Published OnlineFirst January 16, 2014; DOI: 10.1158/1535-7163.MCT-13-0748

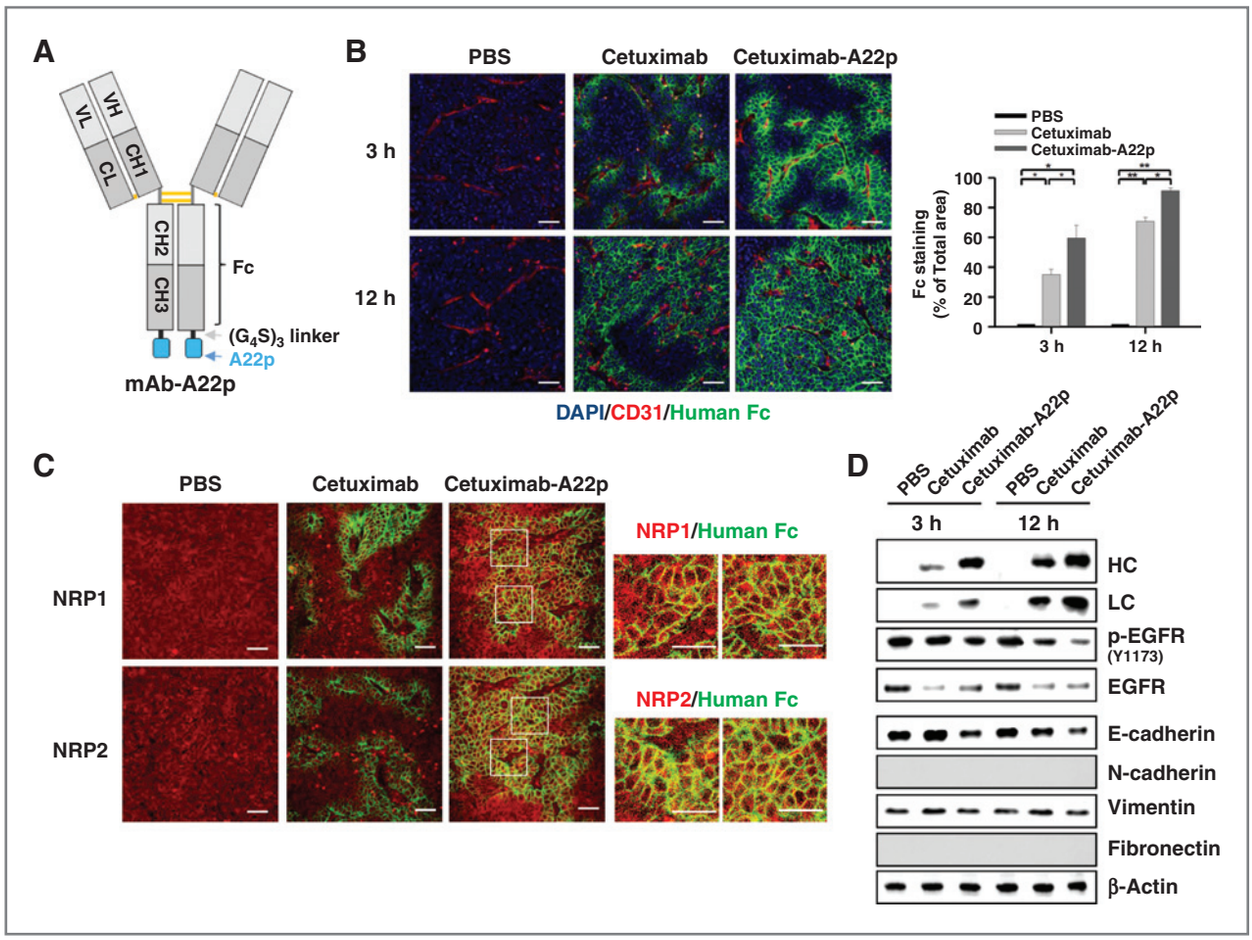

Figure 5. mAb-A22p antibodies exhibit enhanced tumor accumulation and penetration, compared with the parent mAbs. A, the mAb-A22p construct, in which the A22p peptide was fused via a 15-residue $(G_4S)_3$ linker to the C-terminus of antibody heavy chain. B and C, representative images showing the distribution of intravenously injected cetuximab or cetuximab-A22p (2.5 mg/kg) in relation to blood vessels (B) or NRP1 and NRP2 (C) in FaDu xenograft mice, determined by immunofluorescence staining. After the antibodies were circulating for 3 or 12 hours, tumor tissues were excised and subjected to immunofluorescence staining [human Fc (FITC, green), CD31 (TRITC, red), and/or human/mouse NRP1 or NRP2 (TRITC, red)]. Blue represents DAPI staining. Image magnification, ×200; scale bar, 50 μm. In B, right, quantification of the antibody-staining positive areas (green) analyzed by the ImageJ software. Results are the mean ±SD of four fields per tumor ($n = 3$ per group). *, $P < 0.05$; **, $P < 0.001$. D, Western blot analyses of tumor tissue lysates prepared as described in B to compare the amount of human IgG heavy chain (HC) and light chain (LC), phosphorylated EGFR (Y1173), total EGFR, E-cadherin, N-cadherin, vimentin, and fibronectin.

2-fold and 1.5-fold increases at 3 and 12 hours postinjection within the tumors, respectively, compared with the parent mAbs (Fig. 5B; Supplementary Fig. S9A). Similar results were obtained for cetuximab-A22p in EGFR-overexpressing A431 tumor xenografts (Supplementary Fig. S9C). The extravasated cetuximab-A22p, but not cetuximab, colocalized with NRP1/2 in FaDu tumor tissues (Fig. 5C). Quantitative analysis of the antibody levels in tumor lysates by Western blotting also confirmed a greater than 2-fold higher accumulation of mAb-A22p antibodies compared with the parent mAbs (Fig. 5D; Supplementary Fig. S9B). The higher accumulation and farther spreading of cetuximab-A22p could be attributable to the more significant inhibition of EGFR phosphorylation in FaDu tumor tissues, compared with cetuximab (Fig. 5D). Western blots of tumor tissue lysates revealed significant downregulation of E-cadherin at 3 and 12 hours postinjection in the mAb-A22p–injected tumors, but not in the mAb-injected tumors, for both the FaDu and SK-OV-3 xenografts (Fig. 5D; Supplementary Fig. S9B). However, we observed no upregulation of N-cadherin, vimentin, or fibronectin, hallmark proteins associated with tumor invasion and metastasis (35).

mAb-A22p antibodies exhibit superior *in vivo* antitumor efficacy compared with the parent mAbs

To determine whether the enhanced intratumoral accumulation and penetration of mAb-A22p antibodies translates into increased therapeutic efficacy, we compared the *in vivo* antitumor efficacy of the mAb-A22p antibodies with that of the parent mAbs. Antibodies were intravenously administered at 2 different dosages into mice bearing

Published OnlineFirst January 16, 2014; DOI: 10.1158/1535-7163.MCT-13-0748

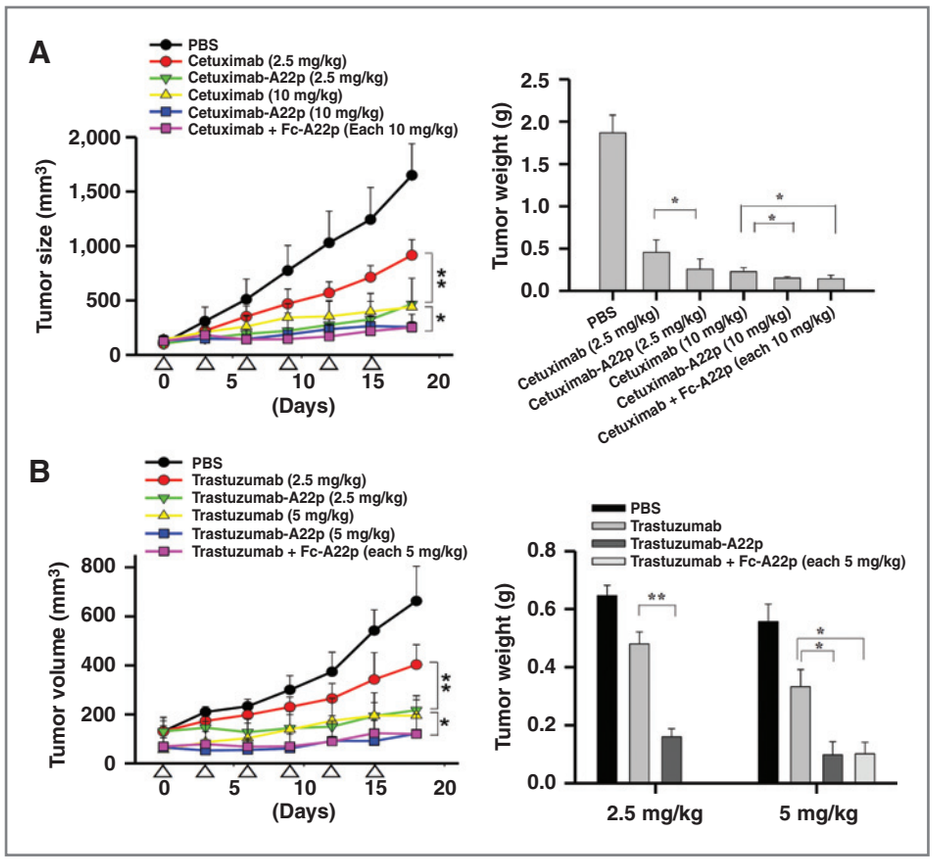

Figure 6. mAb-A22p antibodies exhibit improved antitumor efficacy compared with the parent mAbs. A and B, tumor growth as measured by tumor volume during the treatments (left) and tumor weight at the end of the treatment (right) with cetuximab, cetuximab-A22p, or the combination of cetuximab with Fc-A22p in FaDu xenograft mice (A) or trastuzumab, trastuzumab-A22p, or the combination of trastuzumab with Fc-A22p in SK-OV-3 xenograft mice (B). Mice ($n = 7$ per group) were intravenously injected every 3 days (total = 6 doses; white arrowheads) with the antibodies at the indicated dose. Error bars, ±SD. *, $P < 0.05$; **, $P < 0.001$.

cetuximab-sensitive FaDu tumors for cetuximab or trastuzumab-sensitive SK-OV-3 tumors for trastuzumab. At equivalent dose, the mAb-A22p antibodies exhibited higher antitumor activity from 3 days after the first injection, than the parent mAbs (Fig. 6). The enhanced antitumor efficacy of mAb-A22p antibodies became more prominent at the lower dosage, showing an approximately 2-fold or greater reduction in tumor volume and weight by the end of treatment compared with the parent mAbs. Combined treatments of either cetuximab or trastuzumab with Fc-A22p exhibited similar tumor growth inhibition efficacy to that of the mAb-A22p antibodies but higher than that of the mAbs alone (Fig. 6), indicating that Fc-A22p improves the antitumor efficacy of the coadministered mAbs most likely by enhancing the tumor tissue penetration. Mouse body weight, which was monitored as an indicator of antibody toxicity, was similar between the mAb- and mAb-A22p–treated groups (Supplementary Fig. S9F and S9G).

Discussion

Here, we report the development of a superior solid tumor–targeting antibody format, mAb-A22p, by genetic fusion of high-affinity NRP-targeting A22p peptide to the C-terminus of heavy chain of the conventional mAbs. Due to the bivalent NRP-engaging activity, mAb-A22p antibodies exhibited much better tumor homing, extravasation from blood vessels, and accumulation with deep tissue penetration than the parent mAbs. These properties were directly linked to their superior antitumor efficacy in mouse xenograft models over that of the parent mAbs. Coadministration of mAbs with promoter agents was previously shown to augment the vascular permeability and/or penetration within tumor tissues, which significantly improved the *in vivo* antitumor efficacy (8, 10). However, our approach of directly fusing a tumor-homing and tissue-penetrating peptide to solid tumor–targeting mAbs has not been previously reported.

The molecular mechanism underlying the enhanced tumor homing and tissue penetration of mAb-A22p is mediated by bivalent engagement of cell-surface–expressed NRP1/2, and the mechanism can be dissected into 3 sequential steps (Figs. 1–5): (i) tumor homing by targeting NRP1/2 overexpressed on tumor-associated endothelial cells, (ii) improved extravasation due to enhanced vascular permeability, and (iii) improved tissue penetration by reducing the epithelial barrier. Fc-/mAb-A22p rapidly and extensively localized to tumor vessels compared with the respective parental format, suggesting that NRP1/2 serve as tumor-homing targets due to their overexpression, not only on tumor endothelium, but also on many types of cancer cells (11, 15). Because NRP1/2 are also expressed at low levels in normal tissue vessels (11), however, additional *in vivo* studies to address normal

Published OnlineFirst January 16, 2014; DOI: 10.1158/1535-7163.MCT-13-0748

tissue distribution and any systemic cytotoxicity of Fc-/mAb-A22p are necessary. Fc-A22p enhanced vascular permeability in endothelial cells through NRP-dependent downregulation of VE-cadherin, which explains the enhanced *in vivo* extravasation of Fc-/mAb-A22p into tumor parenchyma. Fc-A22p also penetrated into *ex vivo* tumor tissues, most likely due to the reduced epithelial barrier induced by NRP-mediated downregulation of E-cadherin.

The difference in the antitumor efficacy between SK-OV-3 tumor treatments with trastuzumab-A22p and trastuzumab was more evident (approximately 3-fold) than that between FaDu tumor treatment with cetuximab-A22p and cetuixmab (less than 2-fold) based on the tumor weight (Fig. 6). This could be attributed to the higher expression levels of NRP1/2 in SK-OV-3 cells than those in FaDu cells (Supplementary Fig. S3A). However, the two mAb-A22p antibodies exhibited similarly enhanced levels (approximately 1.5-fold) of tumor tissue penetration compared with the parent mAbs (Fig. 5B and Supplementary Fig. S9). Thus, any relationships between the expression levels of NRPs in tumor cells and the tumor tissue penetration and antitumor efficacy of mAb-A22p antibodies remain to be determined with one set of mAb and mAb-A22p for various tumor cells showing different expression levels of NRP1/2.

Although Fc-A22p acted as an agonist of NRPs triggering its cellular internalization and exerting the biologic activities, the monovalent A22p peptide did not even at 100 μmol/L, suggesting that the bivalent engagement of NRP1/2 by Fc-/mAb-A22p is essential for effective NRP-mediated signaling. Therefore, fusion of the NRP-targeting A22p to the heavy chain C-terminus of mAb seems to induce receptor dimerization by binding to the arginine-binding pocket in the b1 domain of NRP1/2, mimicking the homodimeric binding of VEGF or Sema3 ligands to NRPs (15, 33). VEGF- and Sema3A-induced vascular permeability is commonly dependent on NRP1 coreceptor, but also requires the signal transducing receptor of VEGF-R2 and plexin, respectively (12, 13). Unlike Sema3A, which physically interacts with both NRP1 and plexinA1 receptor (13), Fc-A22p engages only NRP1/2 (Fig. 1F), most likely due to the absence of the additional Sema and Ig-like domains of Sema3A (Supplementary Fig. S1C; ref. 15). Previously, NRP1 promoted vascular permeability independently of VEGF-R2 (37) and the NRP-targeting iRGD peptides enhanced extravascular tumor penetration of coadministered agents (7–9). Along with the previous results, our results suggest that NRP1 and/or NRP2 could transduce the signal to destabilize VE-cadherin and E-cadherin in endothelial and tumor cells, respectively, without its coreceptors. However, at this point we cannot completely exclude the possibility of the interactions of Fc-A22p with additional molecules other than NRP1/2, requiring further studies to clearly elucidate whether NRP1 and/or NRP2 have the independent signaling capacity without any involvement of the coreceptors. Therefore, the intracellular signaling mechanisms triggered by the interactions of Fc-A22p with NRP1/2 need to be elucidated in future studies.

Once extravasated into the tumor parenchyma from blood vessels, mAb-A22p antibodies may bind to NRPs expressed on cancer cells to trigger NRP-mediated E-cadherin downregulation in cell adherens junction, which seems to facilitate the intratumoral penetration and thus the therapeutic efficacy of the antibodies in mouse xenograft tumor models (4). This is similar to that observed with the coadministration of JO-1 viral protein and cetuximab or trastuzumab (10). In the epithelial–mesenchymal transition, tumor cells typically lose the epithelial marker E-cadherin and gain mesenchymal markers, such as vimentin and N-cadherin (35, 36). Treatments with mAb-A22p antibodies only downregulated E-cadherin, but did not upregulate N-cadherin and vimentin in tumor tissues (Fig. 5D; Supplementary Fig. S9B), suggesting that Fc-/mAb-A22p antibodies selectively reduce the epithelial barrier in tumor tissues without promoting invasion and metastasis (35, 36). Nonetheless, additional *in vivo* studies are necessary to determine effects of Fc-/mAb-A22p on the tumor invasion and metastasis.

The mAb-A22p antibodies exhibited biochemical properties comparable with those of the parent mAbs, such as productivity in mammalian cells, antigen binding, and FcRn and FcγRs binding profiles, demonstrating that A22p can be fused to the C-terminal heavy chain of solid tumor–targeting mAbs without compromising their inherent properties. In addition to the direct effects of antigen binding, many anticancer mAbs, including cetuximab and trastuzumab, exert antitumor effects through immune cells, so-called antibody-dependent cell-mediated cytotoxicity (ADCC), in which the interactions between Fc and FcγRs are critical (1). mAb-A22p exhibited comparable FcγR binding properties with those of the parent mAb, suggesting that the ADCC function of mAb-A22p is conserved. The improved accumulation and distribution of mAb-A22p might also enhance the interactions between the mAbs and immune cells to improve their therapeutic efficacy (2). Finally, the superior properties of mAb-A22p antibodies over conventional mAbs include better tumor penetration and improved antitumor efficacy at the same dose, which could potentially reduce resistance and/or relapse of tumors as well as side effects by lowering the therapeutic dose.

Disclosure of Potential Conflicts of Interest

No potential conflicts of interest were disclosed.

Authors' Contributions

Conception and design: T.-H. Shin, E.-S. Sung, Y.-S. Kim
Development of methodology: T.-H. Shin, E.-S. Sung, Y.-J. Kim, S.-H. Kim, Y.-D. Lee, Y.-S. Kim
Acquisition of data (provided animals, acquired and managed patients, provided facilities, etc.): T.-H. Shin, E.-S. Sung, Y.-J. Kim, S.-H. Kim, S.-K. Kim, Y.-D. Lee
Analysis and interpretation of data (e.g., statistical analysis, biostatistics, computational analysis): T.-H. Shin, E.-S. Sung, Y.-J. Kim, Y.-D. Lee, Y.-S. Kim

Published OnlineFirst January 16, 2014; DOI: 10.1158/1535-7163.MCT-13-0748

Writing, review, and/or revision of the manuscript: T.-H. Shin, E.-S. Sung, Y.-J. Kim, Y.-S. Kim
Administrative, technical, or material support (i.e., reporting or organizing data, constructing databases): K.-S. Kim
Study supervision: Y.-S. Kim

Grant Support

This work was supported by grants from the Mid-Career Researcher Program (2013R1A2A2A01005817) and the Converging Research Center Program (2009-0093653; to Y.-S. Kim) from the National Research Foundation, funded by the Korean government.

The costs of publication of this article were defrayed in part by the payment of page charges. This article must therefore be hereby marked *advertisement* in accordance with 18 U.S.C. Section 1734 solely to indicate this fact.

Received September 5, 2013; revised December 15, 2013; accepted January 8, 2014; published OnlineFirst January 16, 2014.

References

1. Scott AM, Wolchok JD, Old LJ. Antibody therapy of cancer. Nat Rev Cancer 2012;12:278–87.
2. Marcucci F, Bellone M, Rumio C, Corti A. Approaches to improve tumor accumulation and interactions between monoclonal antibodies and immune cells. MAbs 2013;5:34–46.
3. Thurber GM, Schmidt MM, Wittrup KD. Antibody tumor penetration: transport opposed by systemic and antigen-mediated clearance. Adv Drug Deliv Rev 2008;60:1421–34.
4. Christiansen J, Rajasekaran AK. Biological impediments to monoclonal antibody-based cancer immunotherapy. Mol Cancer Ther 2004;3:1493–501.
5. Chauhan VP, Stylianopoulos T, Boucher Y, Jain RK. Delivery of molecular and nanoscale medicine to tumors: transport barriers and strategies. Annu Rev Chem Biomol Eng 2011;2:281–98.
6. Beckman RA, Weiner LM, Davis HM. Antibody constructs in cancer therapy: protein engineering strategies to improve exposure in solid tumors. Cancer 2007;109:170–9.
7. Sugahara KN, Teesalu T, Karmali PP, Kotamraju VR, Agemy L, Girard OM, et al. Tissue-penetrating delivery of compounds and nanoparticles into tumors. Cancer Cell 2009;16:510–20.
8. Sugahara KN, Teesalu T, Karmali PP, Kotamraju VR, Agemy L, Greenwald DR, et al. Coadministration of a tumor-penetrating peptide enhances the efficacy of cancer drugs. Science 2010;328:1031–5.
9. Teesalu T, Sugahara KN, Kotamraju VR, Ruoslahti E. C-end rule peptides mediate neuropilin-1-dependent cell, vascular, and tissue penetration. Proc Natl Acad Sci U S A 2009;106:16157–62.
10. Beyer I, van Rensburg R, Strauss R, Li Z, Wang H, Persson J, et al. Epithelial junction opener JO-1 improves monoclonal antibody therapy of cancer. Cancer Res 2011;71:7080–90.
11. Wild JR, Staton CA, Chapple K, Corfe BM. Neuropilins: expression and roles in the epithelium. Int J Exp Pathol 2012;93:81–103.
12. Acevedo LM, Barillas S, Weis SM, Gothert JR, Cheresh DA. Semaphorin 3A suppresses VEGF-mediated angiogenesis yet acts as a vascular permeability factor. Blood 2008;111:2674–80.
13. Le Guelte A, Galan-Moya EM, Dwyer J, Treps L, Kettler G, Hebda JK, et al. Semaphorin 3A elevates endothelial cell permeability through PP2A inactivation. J Cell Sci 2012;125:4137–46.
14. Roth L, Agemy L, Kotamraju VR, Braun G, Teesalu T, Sugahara KN, et al. Transtumoral targeting enabled by a novel neuropilin-binding peptide. Oncogene 2012;31:3754–63.
15. Grandclement C, Borg C. Neuropilins: a new target for cancer therapy. Cancers 2011;3:1899–928.
16. Vander Kooi CW, Jusino MA, Perman B, Neau DB, Bellamy HD, Leahy DJ. Structural basis for ligand and heparin binding to neuropilin B domains. Proc Natl Acad Sci U S A 2007;104:6152–7.
17. Appleton BA, Wu P, Maloney J, Yin J, Liang WC, Stawicki S, et al. Structural studies of neuropilin/antibody complexes provide insights into semaphorin and VEGF binding. EMBO J 2007;26:4902–12.
18. von Wronski MA, Raju N, Pillai R, Bogdan NJ, Marinelli ER, Nanjappan P, et al. Tuftsin binds neuropilin-1 through a sequence similar to that encoded by exon 8 of vascular endothelial growth factor. J Biol Chem 2006;281:5702–10.
19. Maione F, Capano S, Regano D, Zentilin L, Giacca M, Casanovas O, et al. Semaphorin 3A overcomes cancer hypoxia and metastatic dissemination induced by antiangiogenic treatment in mice. J Clin Invest 2012;122:1832–48.
20. Maione F, Molla F, Meda C, Latini R, Zentilin L, Giacca M, et al. Semaphorin 3A is an endogenous angiogenesis inhibitor that blocks tumor growth and normalizes tumor vasculature in transgenic mouse models. J Clin Invest 2009;119:3356–72.
21. Sung ES, Park KJ, Choi HJ, Kim CH, Kim YS. The proteasome inhibitor MG132 potentiates TRAIL receptor agonist-induced apoptosis by stabilizing tBid and Bik in human head and neck squamous cell carcinoma cells. Exp Cell Res 2012;318:1564–76.
22. Song CH, Yang SH, Park E, Cho SH, Gong EY, Khadka DB, et al. Structure-based virtual screening and identification of a novel androgen receptor antagonist. J Biol Chem 2012;287:30769–80.
23. Choi HJ, Kim YJ, Lee S, Kim YS. A heterodimeric Fc-based bispecific antibody simultaneously targeting VEGFR-2 and Met exhibits potent anti-tumor activity. Mol Cancer Ther 2013;12:2748–59.
24. Goldstein NI, Prewett M, Zuklys K, Rockwell P, Mendelsohn J. Biological efficacy of a chimeric antibody to the epidermal growth factor receptor in a human tumor xenograft model. Clin Cancer Res 1995;1:1311–8.
25. Baselga J, Norton L, Albanell J, Kim YM, Mendelsohn J. Recombinant humanized anti-HER2 antibody (Herceptin) enhances the antitumor activity of paclitaxel and doxorubicin against HER2/neu overexpressing human breast cancer xenografts. Cancer Res 1998;58:2825–31.
26. Lee CH, Park KJ, Sung ES, Kim A, Choi JD, Kim JS, et al. Engineering of a human kringle domain into agonistic and antagonistic binding proteins functioning in vitro and in vivo. Proc Natl Acad Sci U S A 2010;107:9567–71.
27. Kim A, Lee JY, Byun SJ, Kwon MH, Kim YS. Viral genome RNA degradation by sequence-selective, nucleic-acid hydrolyzing antibody inhibits the replication of influenza H9N2 virus without significant cytotoxicity to host cells. Antiviral Res 2012;94:157–67.
28. Gavard J, Gutkind JS. VEGF controls endothelial-cell permeability by promoting the beta-arrestin-dependent endocytosis of VE-cadherin. Nat Cell Biol 2006;8:1223–34.
29. Lee CM, Tannock IF. The distribution of the therapeutic monoclonal antibodies cetuximab and trastuzumab within solid tumors. BMC Cancer 2010;10:255.
30. Rhoden JJ, Wittrup KD. Dose dependence of intratumoral perivascular distribution of monoclonal antibodies. J Pharm Sci 2012;101:860–7.
31. Adams RH, Lohrum M, Klostermann A, Betz H, Puschel AW. The chemorepulsive activity of secreted semaphorins is regulated by furin-dependent proteolytic processing. EMBO J 1997;16:6077–86.
32. Parker MW, Xu P, Li X, Vander Kooi CW. Structural basis for the selective vascular endothelial growth factor-A (VEGF-A) binding to neuropilin-1. J Biol Chem 2012;287:11082–9.
33. Salikhova A, Wang L, Lanahan AA, Liu M, Simons M, Leenders WP, et al. Vascular endothelial growth factor and semaphorin induce neuropilin-1 endocytosis via separate pathways. Circ Res 2008;103:e71–9.
34. Dejana E, Orsenigo F, Lampugnani MG. The role of adherens junctions and VE-cadherin in the control of vascular permeability. J Cell Sci 2008;121:2115–22.
35. Kang Y, Massague J. Epithelial-mesenchymal transitions: twist in development and metastasis. Cell 2004;118:277–9.
36. Nasarre P, Kusy S, Constantin B, Castellani V, Drabkin HA, Bagnard D, et al. Semaphorin SEMA3F has a repulsing activity on breast cancer cells and inhibits E-cadherin-mediated cell adhesion. Neoplasia 2005;7:180–9.
37. Becker PM, Waltenberger J, Yachechko R, Mirzapoiazova T, Sham JS, Lee CG, et al. Neuropilin-1 regulates vascular endothelial growth factor-mediated endothelial permeability. Circ Res 2005;96:1257–65.

Published OnlineFirst January 16, 2014; DOI: 10.1158/1535-7163.MCT-13-0748

Molecular Cancer Therapeutics

Enhancement of the Tumor Penetration of Monoclonal Antibody by Fusion of a Neuropilin-Targeting Peptide Improves the Antitumor Efficacy

Tae-Hwan Shin, Eun-Sil Sung, Ye-Jin Kim, et al.

Mol Cancer Ther 2014;13:651-661. Published OnlineFirst January 16, 2014.